Thin-Walled Structures 83 (2014) 115–127

Contents lists available at ScienceDirect

Thin-Walled Structures

journal homepage: www.elsevier.com/locate/tws



# Ultimate response of stainless steel continuous beams

M. Theofanous [a,*], N. Saliba [b], O. Zhao [a], L. Gardner [a]

[a] Department of Civil and Environmental Engineering, Imperial College London, United Kingdom
[b] Department of Civil Engineering, University of Balamand, Lebanon

ARTICLE INFO

Available online 6 February 2014

*Keywords:*
Continuous strength method
Indeterminate structures
Moment redistribution
Plastic design
Stainless steel structures
Tests

ABSTRACT

An experimental study of stainless steel continuous beams not susceptible to lateral torsional buckling is reported in this paper and the applicability of plastic design methods to such structures is considered. A total of 18 two-span continuous beams were tested. Three cross-section types – cold-formed square hollow sections (SHS), cold-formed rectangular hollow sections (RHS) and welded I-sections, and two material grades – austenitic EN 1.4301/1.4307 and lean duplex EN 1.4162, were considered. The geometric and material properties of the continuous beam test specimens were carefully recorded and supplemented by tests on simply supported specimens of the same cross-sections. The test specimens covered a wide range of cross-section slendernesses and two different loading positions were adopted. The experimental results were used to assess the degree of moment redistribution in indeterminate stainless steel structures and the applicability of both conventional and novel plastic design methods, including an extension of the continuous strength method (CSM). Comparisons indicated that conventional plastic design is applicable to stainless steel structures, while greater efficiency can be achieved by considering strain-hardening through the CSM.



## 1. Introduction

Efficient design of metallic structures often involves the exploitation of the inelastic range of the material's stress–strain curve, provided sufficient ductility is available. Modern structural design codes determine the extent to which this exploitation is allowed through the process of cross-section classification. The European structural design codes for carbon steel [1] and stainless steel [2] specify four behavioural classes of cross-sections according to their susceptibility to local buckling. Indeterminate carbon steel structures comprising Class 1 cross-sections classified as Class 1 are assumed to possess sufficient deformation capacity to allow plastic design. However, despite the high material ductility of structural stainless steels [3] and the existence of a Class 1 limit in EN 1993-1-4 [2], plastic design is not currently permitted for stainless steel structures.

The absence of suitable guidance for the design of indeterminate stainless steel structures can be partly attributed to a lack of relevant experimental research. The majority of previously published test data relate to individual stainless steel components rather than complete structures, although some tests on continuous stainless steel beams that allow the assessment of moment redistribution have been reported [4,5]. This paper substantially increases the pool of available test data on indeterminate stainless steel structures, by reporting an experimental investigation on 18 two-span continuous beams. Both cold-formed hollow sections (SHS and RHS) and welded I-sections are examined. Additionally, tests on simply supported beams with the same cross-sections as the continuous beam specimens are reported and the experimental results are utilised in analysing the continuous beam test results. The experimental response of both the simply supported beams and the continuous beams is then compared with the predictions of EN 1993-1-4 [2]. Analysis of the results reveals that current design provisions are overly conservative, since they do not account for material strain-hardening or the significant moment redistribution (in the case of the continuous beams) taking place before collapse. Hence material savings can be achieved if inelastic design procedures are followed at both cross-section level and system level. To this end, the continuous strength method (CSM), originally developed for stainless steel determinate structures [6–8], which allows for the actual material response at cross-sectional level, is adapted to stainless steel indeterminate structures, resulting in more favourable and accurate strength predictions.

## 2. Experimental studies

An experimental investigation into the structural response of stainless steel simple and continuous beams has been carried out in the Structures Laboratory at Imperial College London. The employed cross-sections were SHS and RHS in grade EN 1.4301/

* Corresponding author.
*E-mail address:* m.theofanous@imperial.ac.uk (M. Theofanous).

0263-8231/$ - see front matter © 2014 Elsevier Ltd. All rights reserved.
http://dx.doi.org/10.1016/j.tws.2014.01.019

1.4307 and welded I-sections in grade EN 1.4162. Following material coupon tests, five 3-point bending tests on SHS and RHS, four 3-point bending tests on I-sections and four 4-point bending tests on I-sections were initially performed, to extract fundamental flexural performance data. These were utilised to assess the suitability of current design provisions in EN 1993-1-4 [2]. Subsequently 18 two-span continuous beam tests (five-point bending) were conducted, which enabled the study of stainless steel indeterminate structures and an assessment of the accuracy of current codified provisions. Performing both simply supported and continuous beam tests on the same cross-sections enables the study of the effect of moment redistribution on ultimate capacity of indeterminate structures, since the effect of strain-hardening at cross-sectional level is captured in the 3-point bending tests. A full account of the performed experimental investigations can be found in [9–12].

### 2.1. Material coupon tests

From each of the cold-formed hollow sections employed in the beam tests, both flat and corner coupons were extracted and tested in tension and the key results are summarised in Tables 1 and 2 for flat and corner coupons respectively. Similarly, Table 3 reports the average tensile properties exhibited by the stainless steel plates from which the welded I-sections were fabricated. All tensile tests were conducted in accordance with EN 10002-1 [13]. In Tables 1–3, $E$ is Young's modulus, $\sigma_{0.2}$ is the 0.2% proof stress, $\sigma_{1.0}$ is the 1.0% proof stress, $\sigma_u$ is the ultimate tensile stress, $\varepsilon_f$ is the plastic strain at fracture based on elongation over the standard gauge length ($5.65\sqrt{A_0}$) and $n$ and $n'_{0.2,1.0}$ are strain-hardening exponents for the compound Ramberg–Osgood model [4,14] as modified in [6]. The measured stress–strain curves are reported in [10–12].

### 2.2. Bending tests on simply supported beams

A total of 13 tests on simply supported beams were conducted on the same cross-sections as those employed for the continuous beam tests. The tests were used to quantify the effect of cross-section slenderness on the bending resistance and rotation capacity of the tested beams and to assess the suitability of the European codified slenderness limits as well as revised slenderness limits proposed elsewhere [15]. Moreover the simply supported beam tests were utilised subsequently in the analysis of the continuous beam tests, in order to quantify the relative contribution of strain-hardening at cross-sectional level and moment redistribution at system level to the overstrength displayed by the continuous beams compared to the codified predictions.

**Table 1**
Tensile flat material properties for SHS and RHS.

| Cross-section | $E$ (N/mm$^2$) | $\sigma_{0.2}$ (N/mm$^2$) | $\sigma_{1.0}$ (N/mm$^2$) | $\sigma_u$ (N/mm$^2$) | Modified $R$–$O$ coefficients | |
|---|---|---|---|---|---|---|
| | | | | | $n$ | $n'_{0.2,1.0}$ |
| SHS 50 × 50 × 3 | 198,000 | 552 | 608 | 798 | 5.50 | 2.90 |
| SHS 60 × 60 × 3 | 197,730 | 483 | 546 | 745 | 5.25 | 2.90 |
| SHS 100 × 100 × 3 | 201,300 | 419 | 470 | 725 | 5.25 | 2.25 |
| RHS 60 × 40 × 3 | 191,690 | 538 | 592 | 753 | 5.00 | 3.50 |

**Table 2**
Tensile corner material properties for SHS and RHS.

| Cross-section | $E$ (N/mm$^2$) | $\sigma_{0.2}$ (N/mm$^2$) | $\sigma_{1.0}$ (N/mm$^2$) | $\sigma_u$ (N/mm$^2$) | Modified $R$–$O$ coefficients | |
|---|---|---|---|---|---|---|
| | | | | | $n$ | $n'_{0.2,1.0}$ |
| SHS 50 × 50 × 3 | 195,000 | 723 | 918 | 927 | 4.56 | 3.76 |
| SHS 60 × 60 × 3 | 193,440 | 614 | 776 | 855 | 4.75 | 4.25 |
| SHS 100 × 100 × 3 | 189,520 | 694 | 829 | 839 | 5.50 | 3.50 |
| RHS 60 × 40 × 3 | 198,530 | 741 | 968 | 984 | 4.67 | 4.00 |

**Table 3**
Longitudinal tensile material properties for plates comprising I-sections.

| Nominal plate thickness (mm) | $E$ (N/mm$^2$) | $\sigma_{0.2}$ (N/mm$^2$) | $\sigma_{1.0}$ (N/mm$^2$) | $\sigma_u$ (N/mm$^2$) | Modified $R$–$O$ coefficients | |
|---|---|---|---|---|---|---|
| | | | | | $n$ | $n'_{0.2,1.0}$ |
| 6 | 193,500 | 516 | 557 | 727 | 10.70 | 2.20 |
| 8 | 203,000 | 504 | 545 | 727 | 12.10 | 2.20 |
| 10 | 216,500 | 501 | 557 | 768 | 11.70 | 2.20 |
| 12 | 205,500 | 456 | 506 | 723 | 10.50 | 2.40 |

One test was conducted for each of the three SHS employed in the 3-point bending configuration (Fig. 1), whilst two tests were conducted for the RHS 60 × 40 × 3 specimen, one about the major axis and one about the minor axis. The RHS and SHS beams had a total length of 1200 mm and were simply supported between rollers, which allowed axial displacement of the beams' ends. The rollers were placed 50 mm inward from each beam end. For the RHS 60 × 40 × 3-MA specimen the face containing the weld was the web, whilst in all other cases the face containing the weld was the bottom (tension) flange. A wooden block was inserted at the location of load application to prevent web crippling. All tests were carried out at a rate of 3.0 mm/min. Loads, end rotations, displacements at the points of load application (and at mid-span for the four point bending tests) and strains at a distance of 100 mm from mid-span were all monitored and recorded at one-second intervals using the data acquisition system DATASCAN. Prior to testing, measurements of the geometry of the specimens were taken, which are summarised in Table 4 along with the ultimate moment resistance and the deformation capacity achieved by each specimen. The adopted labelling convention of the cross-section geometry is shown in Fig. 2. The rotation capacity was defined according to Eq. (1), where the $\theta_u$ is the total rotation at mid-span when the moment–rotation curve falls back below the plastic moment capacity $M_{pl}$ as obtained from the test results and $\theta_{pl}$ is the elastic component of the rotation when $M_{pl}$ is reached defined as $\theta_{pl}=M_{pl}L/2EI$ ($I$ being the second moment of area and $L$ the beam length) as shown in Fig. 3. The rotation at mid-span was assumed to equal the sum of the end rotations

$$R=\frac{\theta_u}{\theta_{pl}}-1 \tag{1}$$

All specimens failed by local buckling of the compression flange and the upper part of the web, as shown in Fig. 4. The recorded mid-span moment–rotation (at plastic hinge) responses of the tested beams are depicted in Fig. 5 in a non-dimensional format; the recorded moment has been normalised by the respective plastic moment resistance, while the rotation at plastic hinge has been normalised by $\theta_{pl}$, to facilitate comparison between the specimens.

For each of the four welded I-section geometries considered herein one simply supported beam was tested in the 3-point configuration and one in the 4-point configuration as depicted

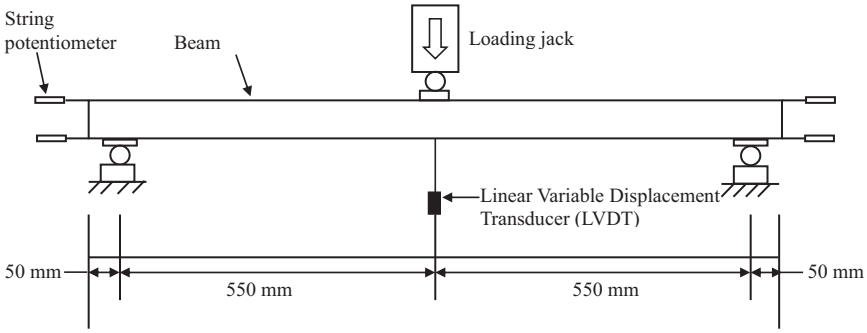


**Fig. 1.** Schematic 3-point bending test arrangement for SHS and RHS.

**Table 4**
Measured dimensions and key results of simply supported SHS and RHS beam tests.

| Specimen | Axis of bending | Width $b$ (mm) | Depth $h$ (mm) | Thickness $t$ (mm) | Root radius $r_i$ (mm) | Ultimate moment $M_u$ (kNm) | Rotation capacity $R$ |
|---|---|---|---|---|---|---|---|
| SHS 50 × 50 × 3 | Major | 50.18 | 50.24 | 2.76 | 1.53 | 7.0 | 3.1[a] |
| SHS 60 × 60 × 3 | Major | 60.37 | 60.63 | 2.79 | 3.50 | 8.7 | 5.3 |
| SHS 100 × 100 × 3 | Major | 99.85 | 99.93 | 2.78 | 2.13 | 18.8 | 1.8 |
| RHS 60 × 40 × 3-MA | Major | 40.00 | 60.11 | 2.75 | 1.88 | 8.0 | 5.1[a] |
| RHS 60 × 40 × 3-MI | Minor | 60.10 | 39.95 | 2.75 | 1.88 | 5.7 | 5.5[a] |

[a] Full rotation capacity not attained; $R$ based on maximum recorded deformation.

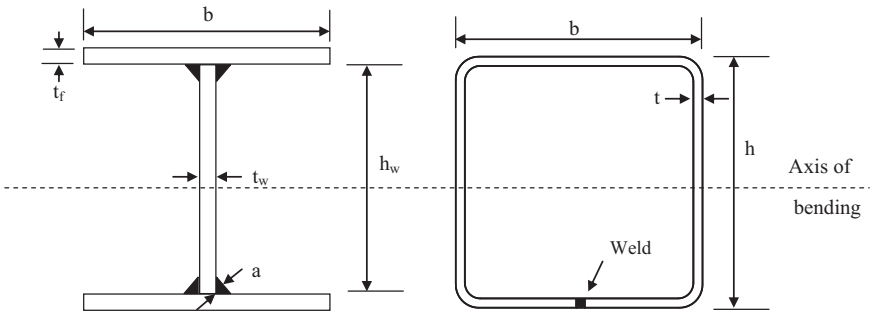


**Fig. 2.** Cross-section notation.

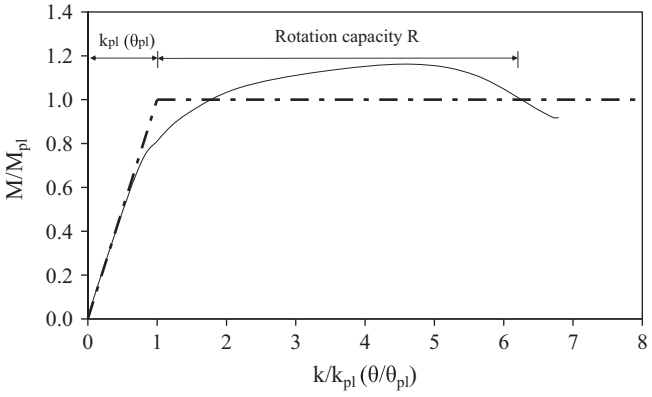


**Fig. 3.** Definition of deformation capacity.

**Fig. 4.** Failure modes for simply supported RHS and SHS beams (from top to bottom: RHS 60 × 40 × 3-MA, RHS 60 × 40 × 3-MI, SHS 50 × 50 × 3, SHS 60 × 60 × 3, SHS 100 × 100 × 3).

schematically in Figs. 6 and 7, where the employed instrumentation is also shown. Each specimen had a total length of 3000 mm and was simply supported between two steel rollers placed 100 mm inwards from the ends of the beams. Lateral restraints were provided at the load points and supports to prevent lateral torsional buckling. The non-dimensional member slenderness of the test specimens $\overline{\lambda}_{LT}$ defined in EN 1993-1-4 [2] varied between 0.29 and 0.34, which is lower than codified limit of 0.4 below which lateral torsional buckling may be ignored. For the 3-point bending tests, the load was applied at mid-span while for the 4-point bending tests the load was applied at two points (900 mm

from each support). For each of the tested beams, web stiffeners were provided at both the end supports and the positions of the applied loads. Displacement rates and data acquisition were as for the SHS/RHS testing. The failure modes of the beams in both the 3-point and 4-point bending tests, exhibiting local buckling of the compression flange and the upper part of the web, are shown in Figs. 8 and 9 respectively, where, in accordance with similar studies [16,17], the local buckling half wavelength in the 3-point bending configuration is shown to be significantly longer than for the 4-point bending configuration. By comparing the results shown in Fig. 10, which displays the moment–rotation response of the welded I-sections, with those in Fig. 5, which shows the response of cold-formed SHS/RHS, it can be observed that the stocky welded-I-sections exhibit a flatter post-yield response with less marked strain-hardening than their cold-formed counterparts of similar slenderness. This is attributed to the different material grades considered, which exhibit different strain-hardening

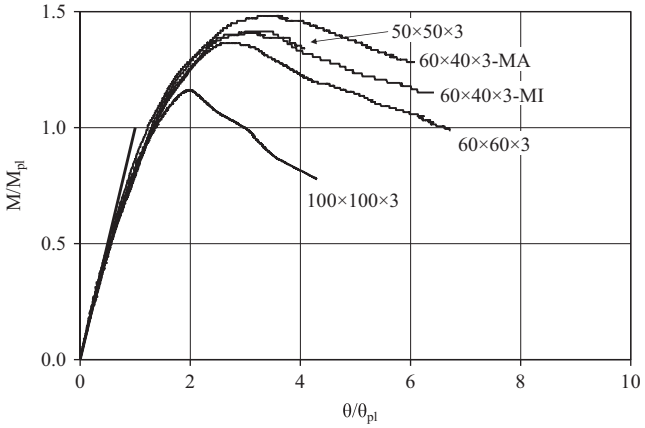


**Fig. 5.** Normalised moment–rotation curves for all specimens.

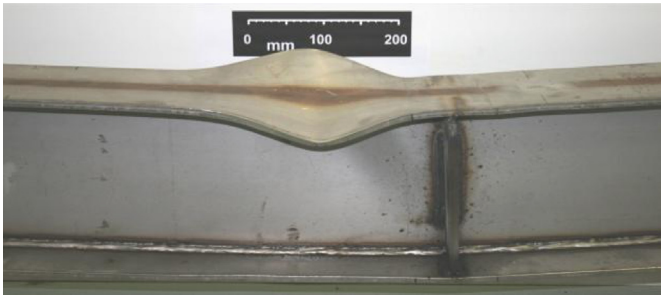


**Fig. 8.** Typical failure mode from 3-point bending tests.

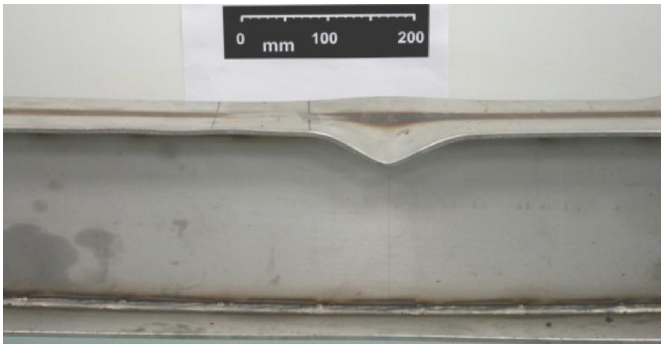


**Fig. 9.** Typical failure mode from 4-point bending tests.

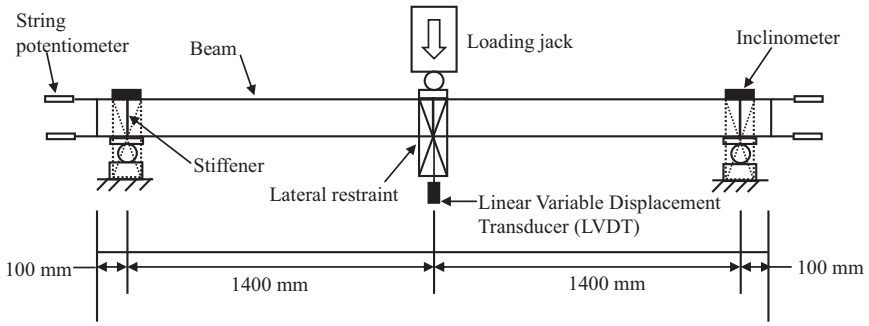


**Fig. 6.** Schematic 3-point bending test arrangement.

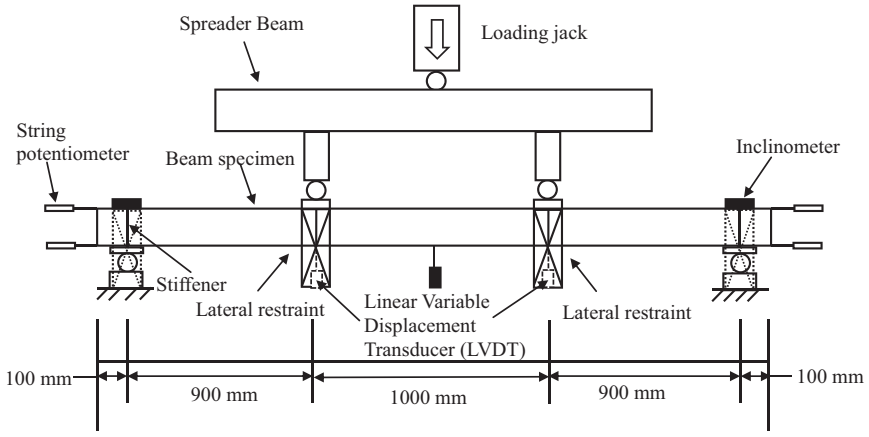


**Fig. 7.** Schematic 4-point bending test arrangement.

**Table 5**
Measured dimensions and key results of simply supported I-section beam tests.

| Specimen | Configuration | Flange width $b$ (mm) | Web depth $h_w$ (mm) | Flange thickness, $t_f$ (mm) | Web thickness $t_w$ (mm) | Weld throat $a$ (mm) | Ultimate moment $M_u$ (kNm) | Rotation capacity $R$ |
|---|---|---|---|---|---|---|---|---|
| I-200 × 140 × 6 × 6-1 | 3-Point bending | 138.89 | 202.05 | 6.12 | 6.01 | 5.0 | 134 | 0.7 |
| I-200 × 140 × 8 × 6-1 | | 139.04 | 200.17 | 8.11 | 6.03 | 5.0 | 195 | 3.8[a] |
| I-200 × 140 × 10 × 8-1 | | 139.00 | 198.72 | 10.18 | 8.00 | 6.0 | 264 | 7.8[a] |
| I-200 × 140 × 12 × 8-1 | | 139.29 | 199.00 | 12.54 | 8.05 | 6.0 | 305 | 7.8[a] |
| I-200 × 140 × 6 × 6-2 | 4-Point bending | 138.60 | 202.05 | 6.11 | 6.01 | 5.0 | 132 | 1.7 |
| I-200 × 140 × 8 × 6-2 | | 139.30 | 200.60 | 8.11 | 6.06 | 5.0 | 169 | 4.6 |
| I-200 × 140 × 10 × 8-2 | | 139.00 | 199.27 | 10.26 | 7.99 | 6.0 | 219 | 14.2 |
| I-200 × 140 × 12 × 8-2 | | 139.64 | 198.87 | 12.32 | 8.07 | 6.0 | 259 | 10.0 |

[a] Full rotation capacity not attained; $R$ based on maximum recorded deformation.

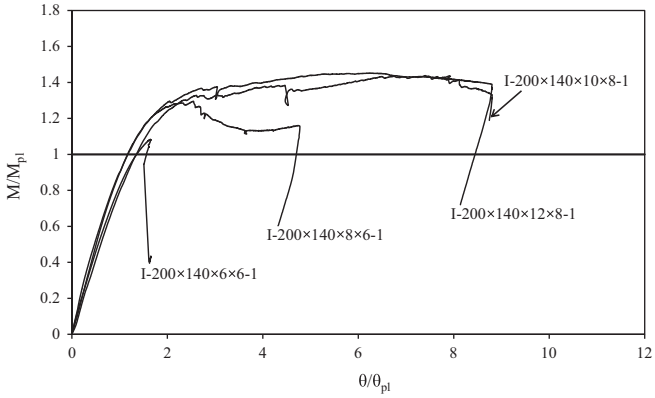


**Fig. 10.** Normalised moment–rotation curves for the tested I-sections sections under 3-point bending.

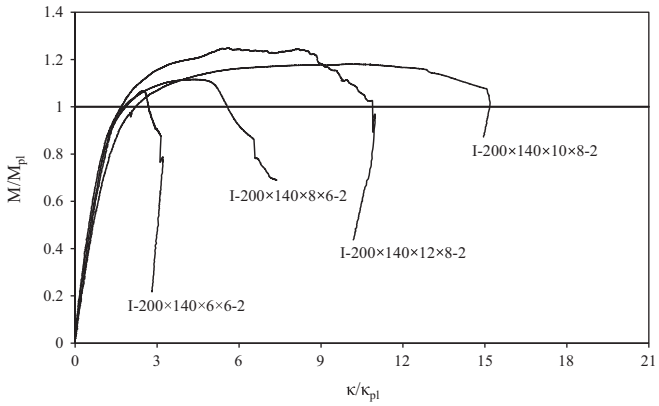


**Fig. 11.** Normalised moment–curvature curves for the tested I-sections sections under 4-point bending.

characteristics, as indicated by the Ramberg–Osgood exponents and $\sigma_{1.0}/\sigma_{0.2}$ ratios summarised in Tables 1–3. Stocky cold-formed austenitic sections display more pronounced strain-hardening and can hence reach higher normalised moments at large rotations than their lean duplex counterparts.

The section dimensions and key experimental results from the beam tests are summarised in Table 5. The deformation capacity is defined in terms of plastic hinge rotation for the 3-point bending tests according to Eq. (1) and in terms of curvature for the 4-point bending tests according to Eq. (2), where $\kappa_u$ is the total curvature at the plastic hinge when the moment–rotation curve falls back below $M_{pl}$, and $\kappa_{pl}$ is the elastic curvature corresponding to $M_{pl}$ defined as $\kappa_{pl}=M_{pl}/EI$. The obtained mid-span moment rotation and moment–curvature curves from the 3-point and 4-point bending tests are shown in Figs. 10 and 11 respectively in a non-dimensional format; the ultimate moment resistance $M_u$ is normalised by the plastic moment capacity $M_{pl}$, the rotation at mid-span taken as the sum of the end rotations $\theta$ is normalised by $\theta_{pl}$, and the curvature $\kappa$ is normalised by $\kappa_{pl}$

$$R=\frac{\kappa_u}{\kappa_{pl}}-1 \tag{2}$$

### 2.3. Continuous beams tests

Eighteen two-span continuous beam tests were conducted on the same section sizes employed for the simply supported beam tests. All tests were displacement-controlled with a loading rate of 3 mm/min in terms of vertical crosshead movement. Two symmetrical loading configurations were employed to vary the required rotation capacity and moment redistribution before collapse. In the first configuration, denoted '1/2 span', the loads were applied at mid-span, whilst in the second configuration, 'denoted 1/3 span', the loads were applied at a distance equal to one-third of the clear span length from the central support. The two configurations are shown in Figs. 12 and 13, where the employed instrumentation is also depicted, which consisted of a load cell at the central support, eight LVDTs and six strain gauges. The load cell was utilised to measure the reaction force at the central support, which is necessary to determine the stress condition of each specimen, due to their statical indeterminacy. The strain gauges were affixed at the mid-width of the top and bottom flanges at a distance of 60 mm from each loading point and from the central support point. Their readings verified that no net axial force was induced in the specimens and hence the end rollers did not provide any axial restraint. Eight LVDTs were employed – two at the ends of the specimens and the central support to measure the end rotations and the rotation of the plastic hinge at the central support, and one at each of the loading points to measure the vertical displacement. The applied load and crosshead movement were also recorded. All readings were taken at 2 s intervals.

The SHS and RHS specimens had a total length of 2400 mm, whilst the total length of the welded I-sections was 5000 mm. All beams were resting on three roller supports; the end rollers allowed free axial displacements, while the central roller was fixed against the axial displacement. The clear span between the roller supports was 1100 mm for the RHS and SHS beams and 2400 mm for the I-section beams, whilst a further 100 mm was provided at each specimen end. Web crippling was prevented by inserting wooden blocks in each of the SHS and RHS specimens and by providing double-sided web stiffeners to the I-sections at the support points and at the loading points. The loads and reactions were applied through a steel block of thickness 15 mm and width 30 mm, to prevent local bearing failure. Similarly to the

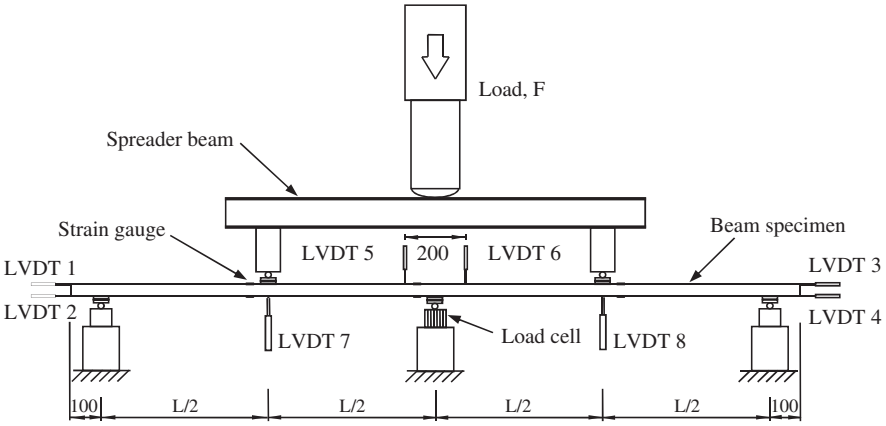


**Fig. 12.** Test configuration '1/2 span' – loads applied at mid-span.

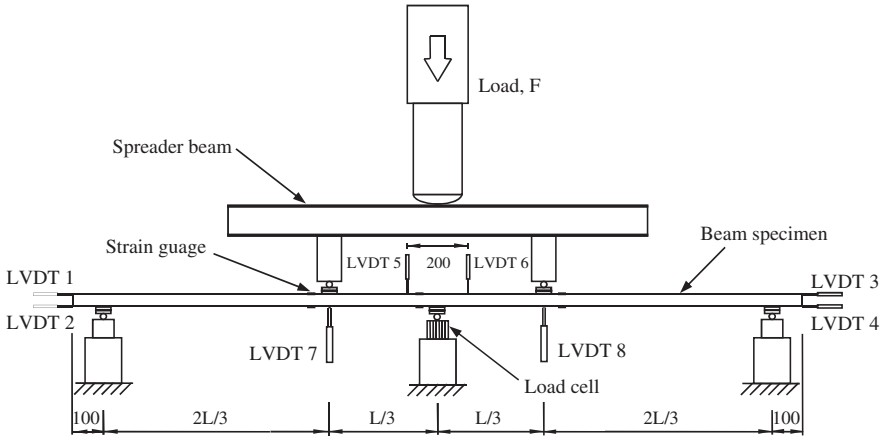


**Fig. 13.** Test configuration '1/3 span' – loads applied at L/3 from central support.

simply supported beam tests, lateral restraints were provided to the I-beams at the support and load points to prevent lateral torsional buckling.

The measured geometric properties and key experimental results are summarised in Tables 6 and 7 for the SHS/RHS and I-sections respectively. As well as the ultimate load at collapse $F_u$, the load corresponding to the formation of the first plastic hinge at the central support, denoted $F_{h1}$, and the theoretical plastic collapse load $F_{coll}$ are also included. It should be noted that these loads refer to the total applied load. The load $F_{h1}$ was determined based on elastic calculations, whereas $F_{coll}$ was determined by classical plastic analysis procedures, assuming rigid-plastic material (and moment–rotation) response. All specimens failed by developing three distinct plastic hinges, one at the central support and one at each loading point. Typical failure modes for both arrangements considered are displayed in Figs. 14 and 15 for SHS/RHS and I-sections respectively. Load–deformation responses are shown in Figs. 16–19, where the total applied load is normalised by the theoretical collapse load $F_{coll}$ reported in Tables 6 and 7 and plotted against average end rotation.

## 3. Analysis of results and assessment of design methods

In this section, the reported test data are analysed and discussed. The applicability and accuracy of a number of design methods are assessed on the basis of the reported results. These include the design provisions specified in EN 1993-1-4 [2], the continuous strength method [6–8], and conventional plastic design, assuming rigid-plastic material behaviour as is customarily applied to carbon steel structures. For the simply supported beams, discrepancies between the actual resistance and code predictions are due to the effect of material nonlinearity (i.e. strain-hardening) at cross-sectional level, while for the continuous beams (indeterminate structures), nonlinearity affects both individual cross-sections, due to material strain-hardening, and the full structural system, due to statical indeterminacy and the corresponding moment redistribution typically achieved in structures comprising stocky cross-sections. Measured geometric and material properties have been used throughout the comparisons, and all partial factors have been set equal to unity.

### 3.1. Cross-section classification

As mentioned earlier, no distinct difference in the treatment of class 1 and class 2 sections exists in EN 1993-1-4 [2], since plastic design of stainless steel indeterminate structures is not currently allowed, despite the existence of a class 1 slenderness limit. Whether a stainless steel structure is determinate, or indeterminate, elastic analysis needs to be applied and plasticity may only be accounted for at cross-sectional level, provided that the cross-section is class 2 or better. Hence failure is assumed to occur when the most heavily stressed cross-section reaches its codified resistance, as determined through cross-section classification, without any allowance for moment redistribution. Exploitation of material strain-hardening is not allowed for, thereby leading to overly conservative ultimate capacity predictions of both determinate and indeterminate stainless steel structures comprising stocky cross-sections. Additional conservatism in EN 1993-1-4 [2] is due to the adopted slenderness limits, which have been shown to be

**Table 6**
Measured dimensions and key results of the continuous SHS and RHS beam tests.

| Specimen | Axis of bending | Configuration | $b$ (mm) | $h$ (mm) | $t$ (mm) | $r_i$ (mm) | $F_u$ (kN) | $F_{h1}$ (kN) | $F_{coll}$ (kN) |
|---|---|---|---|---|---|---|---|---|---|
| SHS 50 × 50 × 3-1 | Major | 1/2 span | 50.22 | 50.26 | 2.76 | 1.38 | 80.2 | 48.3 | 54.4 |
| SHS 50 × 50 × 3-2 | Major | 1/3 span | 50.28 | 50.23 | 2.76 | 1.69 | 98.9 | 48.8 | 67.7 |
| SHS 60 × 60 × 3-1 | Major | 1/2 span | 60.38 | 60.68 | 2.79 | 3.50 | 97.1 | 62.2 | 70.0 |
| SHS 60 × 60 × 3-2 | Major | 1/2 span | 60.36 | 60.66 | 2.79 | 3.50 | 92.5 | 62.2 | 69.9 |
| SHS 100 × 100 × 3-1 | Major | 1/2 span | 99.94 | 99.79 | 2.78 | 2.13 | 173.9 | 156.3 | 175.8 |
| SHS 100 × 100 × 3-2 | Major | 1/2 span | 99.87 | 99.85 | 2.78 | 2.13 | 172.2 | 156.3 | 175.9 |
| RHS 60 × 40 × 3-MA-1 | Major | 1/2 span | 40.05 | 60.14 | 2.75 | 1.88 | 93.0 | 52.0 | 58.5 |
| RHS 60 × 40 × 3-MA-2 | Major | 1/2 span | 39.90 | 60.12 | 2.75 | 1.88 | 91.9 | 51.9 | 58.4 |
| RHS 60 × 40 × 3-MI-1 | Minor | 1/2 span | 60.10 | 39.90 | 2.75 | 1.88 | 63.9 | 39.0 | 43.8 |
| RHS 60 × 40 × 3-MI-2 | Minor | 1/3 span | 60.15 | 39.90 | 2.75 | 1.88 | 77.6 | 39.5 | 54.8 |

**Table 7**
Measured dimensions and key results of the continuous I-section beam tests.

| Cross-section | Configuration | $b$ (mm) | $h_w$ (mm) | $t_f$ (mm) | $t_w$ (mm) | $a$ (mm) | $F_u$ (kN) | $F_{h1}$ (kN) | $F_{coll}$ (kN) |
|---|---|---|---|---|---|---|---|---|---|
| I-200 × 140 × 6 × 6-1 | 1/2 span | 139.22 | 202.40 | 6.07 | 6.02 | 5.0 | 668 | 552 | 620 |
| I-200 × 140 × 8 × 6-1 | | 139.49 | 200.40 | 8.07 | 6.00 | 5.0 | 926 | 668 | 752 |
| I-200 × 140 × 10 × 8-1 | | 139.62 | 199.30 | 10.21 | 8.05 | 5.0 | 1192 | 822 | 924 |
| I-200 × 140 × 12 × 8-1 | | 139.70 | 199.00 | 12.46 | 8.07 | 6.0 | 1474[a] | 934 | 1050 |
| I-200 × 140 × 6 × 6-2 | 1/3 span | 139.20 | 202.60 | 5.99 | 5.98 | 6.0 | 820 | 552 | 766 |
| I-200 × 140 × 8 × 6-2 | | 139.68 | 200.60 | 8.09 | 5.95 | 5.0 | 1062 | 678 | 942 |
| I-200 × 140 × 10 × 8-2 | | 139.59 | 199.10 | 10.2 | 8.07 | 6.0 | 1402[a] | 832 | 1154 |
| I-200 × 140 × 12 × 8-2 | | 139.61 | 198.70 | 12.42 | 8.06 | 6.0 | 1614[a] | 938 | 1302 |

[a] Maximum load not reached due to excessive deformations; $F_u$ based on maximum recorded load

**Fig. 14.** Failure modes of SHS 50 × 50 × 3-1 – configuration: 1/2 span (top) and SHS 50 × 50 × 3-2 – configuration: 1/3 span (bottom).

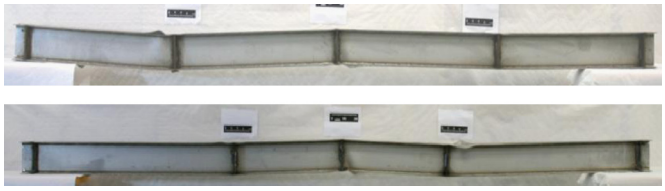

**Fig. 15.** Typical failure modes of I-200 × 140 × 6 × 6-1 – configuration: 1/2 span (top) and I-200 × 140 × 8 × 6-2 – configuration: 1/3 span (bottom).

overly stringent and could be relaxed based on the available test data [15]. Moreover, in the case of the SHS and RHS, the significant strength enhancements in the corner regions brought about by the cold forming process [18–20] are not explicitly accounted for, thereby further increasing conservatism. It should be noted that even though the increased strength of the flat parts of the cold-formed SHS and RHS is not allowed for in EN 1993-1-4 [2], it is implicitly included in this paper since all material properties have been obtained from tensile tests on coupons extracted from the finished cross-sections.

The codified ultimate capacity predictions based on the slenderness limits and effective width formulae of EN 1993-1-4 [2] are assessed on the basis of the reported test data in Tables 8 and 9 for the simply supported and continuous beams respectively. The predictions based on proposed revised slenderness limits and

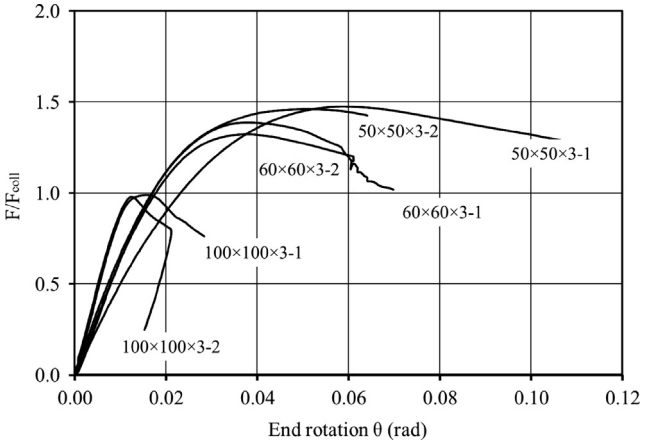


**Fig. 16.** Normalised load-end rotation curves SHS continuous beams.

effective width formulae [15] and those based on the continuous strength method (discussed in the following subsection) are also included for comparison. On average, EN 1993-1-4 [2] underestimates the capacity of the simply supported beams by 28% with a COV of 9%. Slightly improved results in terms of consistency and efficiency are obtained when the calculations are based on the revised slenderness limits and effective width formulae, where the

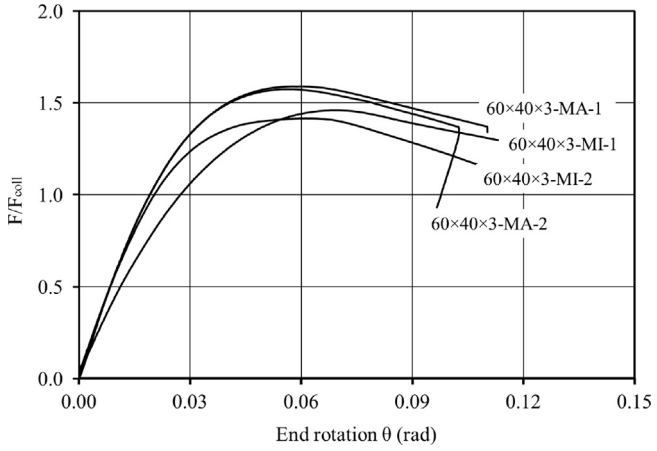


**Fig. 17.** Normalised load-end rotation curves RHS continuous beams.

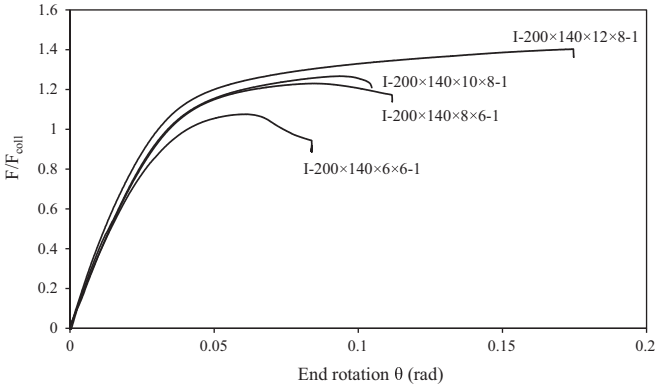


**Fig. 18.** Normalised load versus end rotation for I-beams tested in the 1/2 span configuration.

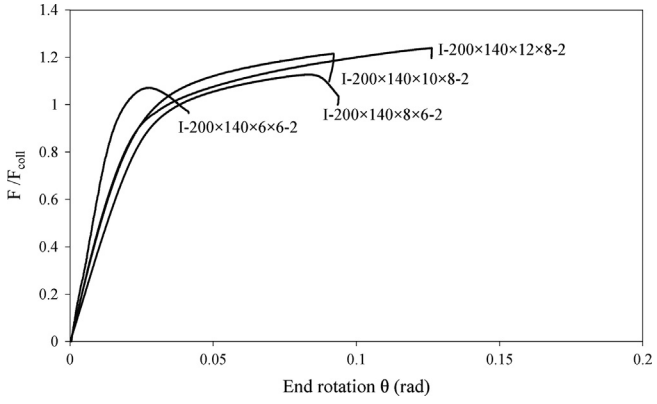


**Fig. 19.** Normalised load versus end rotation for I-beams tested in the 1/3 span configuration.

capacity is underestimated by 26% and the COV is 8%. A higher conservatism can be observed for the SHS and RHS, due to the fact that the corner strength enhancements have not been taken into account. Similar observations can be made for the continuous beams in Table 9, where, as expected, the conservatism is higher, since as well as the strain-hardening at cross-sectional level, the moment redistribution exhibited by indeterminate structures employing stocky cross-sections is also not taken into account.

### 3.2. The continuous strength method

Current design provisions have been shown to significantly underestimate the capacity of stocky stainless steel cross-sections as they fail to account for the material strain-hardening [3–11,15]. To address this shortcoming the continuous strength method (CSM) has been developed and statistically validated as an alternative design approach that rationally exploits material strain-hardening at the cross-sectional level. It is essentially a strain based design approach that employs a 'base curve' to determine the strain that a cross-section can sustain, in conjunction with a material model that allows for strain hardening, to determine section resistance. The maximum attainable strain $\varepsilon_{csm}$ by a cross-section prior to the occurrence of local buckling is given as a function of local slenderness by Eq. (3), for cross-sections with $\bar{\lambda}_p \le 0.68$; more slender cross-sections lie beyond the scope of the CSM and should be designed with the aid of the revised effective width formulae [15] or the direct strength method (DSM) [21]

$$\frac{\varepsilon_{csm}}{\varepsilon_y} = \frac{0.25}{\bar{\lambda}_p^{3.6}} \quad \text{but} \le \min\left\{15; \frac{0.1\varepsilon_u}{\varepsilon_y}\right\} \quad \text{for } \bar{\lambda}_p \le 0.68 \tag{3}$$

where $\varepsilon y = fy/E$ is the yield strain and $\varepsilon u = 1 - fy/fu$ is the strain at the ultimate tensile stress. The non-dimensional cross-sectional slenderness $\bar{\lambda}_p$ is defined by the following equation:

$$\bar{\lambda}_p = \sqrt{\frac{f_y}{f_{cr}}} \tag{4}$$

where $f_{cr}$ is the critical buckling stress corresponding to the lowest (local) buckling mode pertaining to the loading case considered, which can be obtained by eigenvalue buckling analysis using a finite element or finite strip analysis. In this paper the software CUFSM [22,23] was utilised to obtain the critical buckling stresses. Conservatively, cross-section slenderness could also be calculated on the basis of the most slender plate element in the cross-section, in accordance with the provisions of [2,24]. The resulting slenderness value given by Eq. (4) may be further refined by multiplying it by the maximum flat width to mid-line width ratio of the constituent plate elements; this adjustment accounts for the fact that only the flat width of the constituent plate elements may buckle locally, whereas the root radii remain undeformed.

Having established the maximum strain that can be reached by the cross-section and assuming a linear strain distribution for cross-sections subjected to bending (i.e. planarity of the cross-section) the corresponding stress distribution at failure can be obtained. The adopted material model is of the elastic-strain hardening form shown in Fig. 20. The strain-hardening slope $E_{sh}$ is given by Eq. (5), whilst the ultimate moment resistance $M_{csm}$ for an RHS or an I-section subjected to major axis bending can be obtained from Eq. (6) [25]. A detailed account of the latest developments to the CSM can be found in [26]

$$E_{sh} = \frac{f_u - f_y}{0.16\varepsilon_u - \varepsilon_y} \tag{5}$$

$$\frac{M_{csm}}{M_{pl}} = 1 + \frac{E_{sh}}{E}\frac{W_{el}}{W_{pl}}\left(\frac{\varepsilon_{csm}}{\varepsilon_y} - 1\right) - \left(1 - \frac{W_{el}}{W_{pl}}\right)\left(\frac{\varepsilon_{csm}}{\varepsilon_y}\right)^{-2} \tag{6}$$

Since the CSM explicitly accounts for material strain-hardening at cross-sectional level, more favourable ultimate capacity predictions can be achieved for both simply supported and continuous beams if the cross-section resistance is based on the CSM rather than on cross-section classification, as shown in Tables 8 and 9 for simply supported and continuous beams respectively. For the SHS/RHS, the effect of the enhanced corner strength has been explicitly accounted for according to the provisions given in [19].

On average, the ultimate capacity of the simply supported beams is underpredicted by the CSM by 10% with a COV of 0.09, as shown in Table 8. For the continuous beams, the CSM gives more favourable strength predictions compared to the classification procedures, but failure to account for moment redistribution

**Table 8**
Assessment of design methods for simply supported beams.

| Specimen | EN 1993-1-4 (2006) | | Revised slenderness limits | | CSM | | | |
|---|---|---|---|---|---|---|---|---|
| | Class | $M_{pred}/M_u$ | Class | $M_{pred}/M_u$ | $\overline{\lambda}_p$ | $\varepsilon_{csm}/\varepsilon_y$ | $E_{sh}$ (MPa) | $M_{pred}/M_u$ |
| SHS 50 × 50 × 3 | 1 | 0.71 | 1 | 0.71 | 0.35 | 10.8 | 5286 | 0.97 |
| SHS 60 × 60 × 3 | 1 | 0.73 | 1 | 0.73 | 0.37 | 9.0 | 4868 | 0.95 |
| SHS 100 × 100 × 3 | 4 | 0.65 | 4 | 0.68 | 0.66 | 1.1 | 4675 | 0.81 |
| RHS 60 × 40 × 3-MA | 1 | 0.67 | 1 | 0.67 | 0.28 | 15.0 | 5014 | 0.90 |
| RHS 60 × 40 × 3-MI | 3 | 0.60 | 1 | 0.71 | 0.42 | 5.7 | 5014 | 0.86 |
| I-200 × 140 × 6 × 6-1 | 4 | 0.72 | 4 | 0.76 | 0.65 | 1.2 | 4821 | 0.85 |
| I-200 × 140 × 8 × 6-1 | 4 | 0.69 | 3 | 0.70 | 0.51 | 2.7 | 4798 | 0.79 |
| I-200 × 140 × 10 × 8-1 | 1 | 0.69 | 1 | 0.69 | 0.38 | 8.5 | 4924 | 0.83 |
| I-200 × 140 × 12 × 8-1 | 1 | 0.69 | 1 | 0.69 | 0.31 | 15.0 | 4722 | 0.90 |
| I-200 × 140 × 6 × 6-2 | 4 | 0.73 | 4 | 0.77 | 0.65 | 1.2 | 4821 | 0.86 |
| I-200 × 140 × 8 × 6-2 | 4 | 0.79 | 3 | 0.81 | 0.51 | 2.7 | 4798 | 0.91 |
| I-200 × 140 × 10 × 8-2 | 1 | 0.85 | 1 | 0.85 | 0.37 | 8.9 | 4924 | 1.00 |
| I-200 × 140 × 12 × 8-2 | 1 | 0.80 | 1 | 0.80 | 0.31 | 15.0 | 4722 | 1.06 |
| Mean | | 0.72 | | 0.74 | | | | 0.90 |
| COV | | 0.09 | | 0.08 | | | | 0.09 |

**Table 9**
Assessment of design methods based on elastic analysis for continuous beams.

| Specimen | EN 1993-1-4 (2006) | | Revised slenderness limits | | CSM |
|---|---|---|---|---|---|
| | Class | $F_{pred}/F_u$ | Class | $F_{pred}/F_u$ | $M_{pred}/M_u$ |
| SHS 50 × 50 × 3-1 | 1 | 0.60 | 1 | 0.60 | 0.81 |
| SHS 50 × 50 × 3-2 | 1 | 0.49 | 1 | 0.49 | 0.67 |
| SHS 60 × 60 × 3-1 | 1 | 0.64 | 1 | 0.64 | 0.83 |
| SHS 60 × 60 × 3-2 | 1 | 0.67 | 1 | 0.67 | 0.87 |
| SHS 100 × 100 × 3-1 | 4 | 0.68 | 4 | 0.71 | 0.85 |
| SHS 100 × 100 × 3-2 | 4 | 0.68 | 4 | 0.72 | 0.85 |
| RHS 60 × 40 × 3-MA-1 | 1 | 0.56 | 1 | 0.56 | 0.75 |
| RHS 60 × 40 × 3-MA-2 | 1 | 0.56 | 1 | 0.56 | 0.75 |
| RHS 60 × 40 × 3-MI-1 | 3 | 0.52 | 1 | 0.61 | 0.75 |
| RHS 60 × 40 × 3-MI-2 | 3 | 0.43 | 1 | 0.51 | 0.62 |
| I-200 × 140 × 6 × 6-1 | 4 | 0.64 | 4 | 0.68 | 0.76 |
| I-200 × 140 × 8 × 6-1 | 4 | 0.65 | 3 | 0.66 | 0.74 |
| I-200 × 140 × 10 × 8-1 | 1 | 0.70 | 1 | 0.70 | 0.81 |
| I-200 × 140 × 12 × 8-1 | 1 | 0.64 | 1 | 0.64 | 0.83 |
| I-200 × 140 × 6 × 6-2 | 4 | 0.53 | 4 | 0.56 | 0.62 |
| I-200 × 140 × 8 × 6-2 | 4 | 0.57 | 3 | 0.57 | 0.65 |
| I-200 × 140 × 10 × 8-2 | 1 | 0.60 | 1 | 0.60 | 0.70 |
| I-200 × 140 × 12 × 8-2 | 1 | 0.59 | 1 | 0.59 | 0.77 |
| Mean | | 0.60 | | 0.61 | 0.76 |
| COV | | 0.12 | | 0.11 | 0.10 |

still results in conservatism, as evidenced in Table 9, where a mean value of the ratio of predicted to experimental capacity of 0.76 is observed. Hence, it can be concluded that the CSM adequately predicts cross-section resistance, but requires refinement to allow for moment redistribution. The application of plastic design to stainless steel continuous beams is examined hereafter.

### 3.3. Plastic design

In plastic design, unlike conventional elastic design, failure is defined by the formation of a mechanism of plastic hinges at ultimate load, thereby allowing redistribution of bending moments and the exploitation of the structure's reserve strength due to statical indeterminacy. The structure is generally assumed to behave elastically up to the formation of the first plastic hinge upon which, the hinge is assumed to rotate freely maintaining its plastic moment capacity and allowing moment redistribution to other parts of the structure until a sufficient number of hinges form and the structure collapses. Since it was originally devised for carbon steel structures, plastic analysis is based on the adoption of an elastic, perfectly plastic material response. The analysis procedure is significantly simplified by assuming rigid-plastic material behaviour and utilising the classical theorems of plasticity (i.e. upper bound theorem, lower bound theorem, uniqueness theorem). Sufficient cross-section rotation capacity is required at the location of the plastic hinges, since the plastic hinges are assumed to maintain their strength while undergoing large rotations, until the collapse mechanism forms. Hence, ductility i.e. the ability of a material or cross-section to undergo large inelastic deformation without significant loss of strength, emerges as a key property for plastic design.

Despite the deviation of stainless steel's material response from the assumed bilinear elastic, perfectly plastic model, application of plastic design to stainless steel indeterminate structures is considered herein. The theoretical collapse load $F_{coll}$ has been calculated assuming rigid plastic material response for all continuous beam specimens and is given in Tables 6 and 7 for the SHS/RHS and I-section continuous beams respectively. The predicted collapse load for the SHS/RHS and I-section specimens has been normalised by the ultimate capacity obtained experimentally and plotted against the cross-section slenderness obtained from Eq. (4) in Fig. 21. Note that, for comparison purposes, plastic design has been applied to all test specimens, regardless of the cross-section slenderness and, as expected, the capacity of the most slender specimens is overpredicted. The results indicate that plastic design provides safe predictions of the resistance of stainless steel continuous beams with stocky cross-sections, whereas conservatism decreases with increasing cross-section slenderness. In Table 10, test and calculated resistances for the tested continuous beams using the EN 1993-1-4 [2] and the proposed slenderness limits [15] are again assessed on the following basis: the capacity of the specimens with Class 1 cross-sections is calculated by means of plastic design, the resistance of the Class 3 beams is calculated using elastic design and for the Class 4 beams, elastic design and effective section properties are used. The revised classification approach seems to offer more consistent ultimate capacity predictions than that of EN 1993-1-4 [2]. However the embedded conservatism remains significant, since only spread of yielding throughout stocky cross-sections is allowed, whereas strain-hardening at cross-sectional level is not accounted for.

## 4. The continuous strength method for indeterminate structures

Stainless steel indeterminate structures with stocky cross-sections possess high deformation capacity, and moment

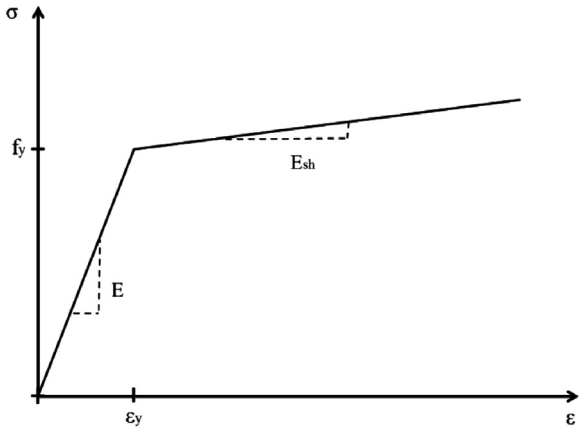


**Fig. 20.** Bilinear elastic-strain hardening material model.

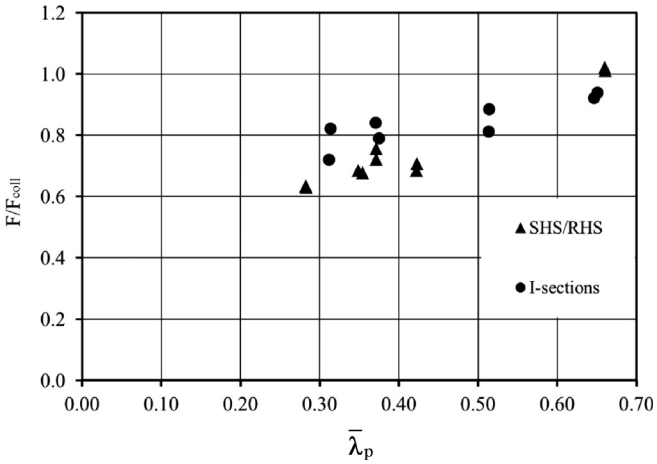


**Fig. 21.** Assessment of conventional plastic design.

**Table 10**
Assessment of codified and proposed classification and effective width formulae for continuous beams allowing for plastic design.

| Specimen | EN 1993-1-4 (2006) | | Revised slenderness limits | |
|---|---|---|---|---|
| | Class | $F_{pred}/F_u$ | Class | $F_{pred}/F_u$ |
| SHS 50 × 50 × 3-1 | 1 | 0.68 | 1 | 0.68 |
| SHS 50 × 50 × 3-2 | 1 | 0.68 | 1 | 0.68 |
| SHS 60 × 60 × 3-1 | 1 | 0.72 | 1 | 0.72 |
| SHS 60 × 60 × 3-2 | 1 | 0.76 | 1 | 0.76 |
| SHS 100 × 100 × 3-1 | 4 | 0.68 | 4 | 0.71 |
| SHS 100 × 100 × 3-2 | 4 | 0.68 | 4 | 0.72 |
| RHS 60 × 40 × 3-MA-1 | 1 | 0.63 | 1 | 0.63 |
| RHS 60 × 40 × 3-MA-2 | 1 | 0.63 | 1 | 0.63 |
| RHS 60 × 40 × 3-MI-1 | 3 | 0.52 | 1 | 0.69 |
| RHS 60 × 40 × 3-MI-2 | 3 | 0.43 | 1 | 0.71 |
| I-200 × 140 × 6 × 6-1 | 4 | 0.64 | 4 | 0.68 |
| I-200 × 140 × 8 × 6-1 | 4 | 0.65 | 3 | 0.66 |
| I-200 × 140 × 10 × 8-1 | 1 | 0.79 | 1 | 0.79 |
| I-200 × 140 × 12 × 8-1 | 1 | 0.72 | 1 | 0.72 |
| I-200 × 140 × 6 × 6-2 | 4 | 0.53 | 4 | 0.56 |
| I-200 × 140 × 8 × 6-2 | 4 | 0.57 | 3 | 0.57 |
| I-200 × 140 × 10 × 8-2 | 1 | 0.84 | 1 | 0.84 |
| I-200 × 140 × 12 × 8-2 | 1 | 0.82 | 1 | 0.82 |
| Mean | | 0.66 | | 0.70 |
| COV | | 0.16 | | 0.11 |

redistribution will occur prior to collapse regardless of whether or not such an assumption is made in the design. Furthermore, moment redistribution may cause joints to be subjected to higher moments than the ones for which they have been designed. Hence, better prediction of the actual response of stainless steel indeterminate structures is necessary for both safe and economic designs to be achieved.

From the presented analysis, the significance of material non-linearity for stainless steel indeterminate structures both at cross-section and at system level has been revealed. The current design approach of EN 1993-1-4 [2] accounts for neither and therefore leads to overly conservative strength predictions, particularly for stainless steel indeterminate structures with stocky cross-sections. Improved capacity predictions are obtained when either material strain-hardening or moment redistribution is accounted for. The development of a method combining the merits of both is desirable, since both strain-hardening at cross-sectional level and moment redistribution affect the structural response of stainless steel indeterminate structures. A method for plastic design of carbon steel structures, which takes into account strain-hardening, was recently proposed in [25] and its applicability to stainless steel indeterminate structures is assessed herein.

### 4.1. Outline of the method

A modification to the traditional plastic analysis procedure currently applied to carbon steel structures was recently proposed [25], and verified using experimental results of both hot-rolled and cold-formed continuous beams [27]. The method, called the CSM for indeterminate structures, allows for moment redistribution in a similar fashion to traditional plastic analysis and for exploitation of material strain-hardening. The full CSM cross-section resistance is assigned at the location of the critical plastic hinge (i.e. the plastic hinge subjected to the largest rotation demand), while a degree of strain-hardening is also allowed for at subsequent hinges. In essence, the method utilises the upper bound theorem of limit analysis and relies on the determination of a suitable collapse mechanism. The novelty of the method lies in adopting an elastic-linear hardening material response, as shown in Fig. 20, rather than the traditional rigid-plastic material response, thereby allowing for strain-hardening at cross-sectional level and moments larger than the plastic moment resistance to be attained by stocky cross-sections.

For a given structural configuration all possible collapse mechanisms (i.e. location and relative rotation of the plastic hinges) have to be identified in a manner similar to traditional plastic design. For illustration purposes, Fig. 22 depicts a typical collapse mechanism pertinent to a two-span continuous beam loaded with point loads. For each collapse mechanism, the rotation demand $\alpha_i$ of each of the $i$ hinges is determined according to the following equation:

$$\alpha_i = \frac{\theta_i h_i}{(\varepsilon_{csm}/\varepsilon_y)_i} \tag{7}$$

where $\theta_i$ is the relative rotation derived from kinematics considerations for the collapse mechanism considered, $h_i$ is the section height at the considered location and $(\varepsilon_{csm}/\varepsilon_y)_i$ is the corresponding normalised strain ratio at the $i$th hinge. The critical plastic hinge is identified as the one that undergoes the greatest deformation demand $\alpha_{crit}$ relative to the deformation capacity of the cross-section at that location $(\varepsilon_{csm}/\varepsilon_y)_{crit}$; the deformation capacity is given by Eq. (3) in terms of strains. In cases of constant section sizes, the critical hinge is simply the one that undergoes maximum rotation, as limited by its deformation capacity. The deformation demands in terms of strains at other plastic hinge locations are then assigned relative to that of the critical hinge, according to the

following equation:

$$\left(\frac{\varepsilon_{csm}}{\varepsilon_y}\right)_i = \frac{\alpha_i}{\alpha_{crit}}\left(\frac{\varepsilon_{csm}}{\varepsilon_y}\right)_{crit} \leq \left(\frac{\varepsilon_{csm}}{\varepsilon_y}\right)_i \quad (8)$$

Based on the resulting strain demands, the corresponding moment capacities at the location of the plastic hinges are calculated by means of the CSM. For the first plastic hinge, the full deformation capacity is exploited, while for subsequent plastic hinges, deformations are reduced in proportion to the plastic hinge rotations ratio, as determined from kinematics. This is illustrated in Fig. 23 where a typical moment–rotation response for a plastic hinge is depicted. At the plastic hinge associated with the greatest deformation demand, the full bending moment $M_{csm}$ is attained at the rotation $\theta_{csm}$, while the moment $M_i$ at each subsequent plastic hinge location is determined on the basis of the ratio of the rotation $\theta_i$ to $\theta_{csm}$ as determined from the collapse mechanism considered. Hence, following this procedure, the bending moment diagram at collapse is obtained. Finally the collapse load is determined by equating the external work done by the applied loads to the internal work resulting from rotation of the plastic hinges, as in conventional plastic design. The mechanism yielding the lowest collapse load is the critical collapse mechanism for the structure considered.

Clearly, sufficient deformation capacity must be available for moment redistribution to occur in stainless steel indeterminate structures. EN 1993-1-1 [1] is based on a minimum rotation capacity of $R=3$ [28,29]. This rotation capacity is assumed to be possessed by Class 1 cross-sections. However in the case of stainless steel structures, the relevance of this rotation capacity $R$, which is defined on the basis of a cross-section being able to attain its plastic moment resistance $M_{pl}$, is less clear. Hence, instead the deformation capacity adopted herein relates to the maximum attainable strain $\varepsilon_{csm}$, as given by Eq. (3). In accordance with [25] a minimum $\varepsilon_{csm}/\varepsilon_y$ value for the critical plastic hinge of 3 for I-sections and 3.6 for box sections is assumed as the limiting (minimum) value for moment redistribution to be considered.

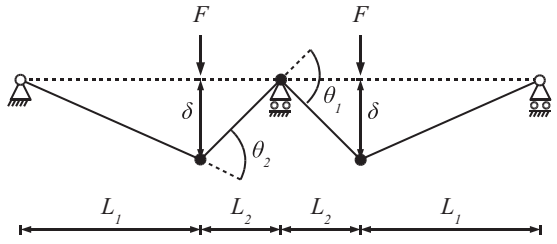


**Fig. 22.** Typical collapse mechanism for a two-span continuous beam.

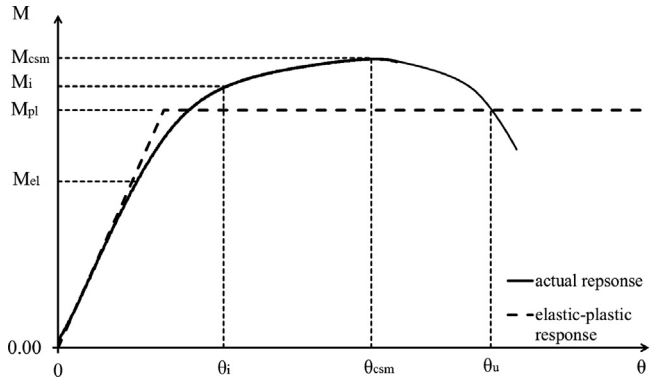


**Fig. 23.** Typical moment–rotation response of a plastic hinge.

### 4.2. Assessment of the method

The CSM for indeterminate structures has been applied to the continuous beams tested in this study. Its accuracy is assessed in Table 11, where the predicted collapse load $F_{pred}$ is normalised by the experimentally obtained collapse load $F_u$. The normalised deformation capacity $\varepsilon_{csm}/\varepsilon_y$, as well as the classification according to the revised slenderness limits [15], is also included. On average the experimental capacity is underpredicted by 9% with a COV of 6%. This constitutes a significant improvement compared to all other design methods which have been assessed in Tables 9 and 10 in terms of both design efficiency and consistency of the predictions. It should also be noted that on average the CSM for indeterminate structures displays similar conservatism to the CSM for determinate structures, as shown in Table 8 for the simply supported beams. The higher COV observed for determinate structures is attributed to the effect of the moment gradient on moment resistance, which is not accounted for by any design method. This suggests that the CSM for indeterminate structures adequately addresses the issue of moment redistribution.

Similar conclusions to those described above are also drawn by analysing the test results of the six two-span stainless steel continuous beams reported by Mirambell and Real [4,5]. The described design methods are assessed on the basis of these test results in Tables 12 and 13, for design procedures based on elastic analysis and plastic analysis respectively.

### 4.3. Discussion

A key assumption underlying the CSM for indeterminate structures is that the required deformation capacity at the plastic hinges at collapse can be determined from the ratio of the plastic hinge rotations assuming a rigid plastic collapse mechanism. For example, for the '1/2 span' configuration the kinematics imply that, at collapse, the bending moment at the central support should be equal to the bending moments at the spans since the hinge rotations are equal. During the experimental study, both the total applied load and the reaction at the central support have been monitored and recorded. Hence, taking into account the symmetry of the structure, the reactions at the end supports can be obtained, and thus the bending moment diagram for each beam can be derived from the recorded test data for each increment of the loading history and utilised to assess the validity of this assumption.

In Fig. 24, the experimentally derived ratio of the central support moment to the span moment $M_{support}/M_{span}$ is plotted against the jack displacement for the SHS $50\times50\times3$-1 specimen tested in the '1/2 span' configuration. The theoretical moment ratios are 1.2 and 1.0 for elastic analysis and rigid plastic analysis respectively. These limits have been plotted with horizontal dotted lines, while the vertical dotted line passes through the displacement value at which collapse (i.e. ultimate load) occurred. The experimentally derived moment ratio may be seen to be equal to the elastic ratio at the early stages of loading and migrates towards the plastic ratio following yielding, spread of plasticity and subsequent moment redistribution with increasing jack displacement. Similar behaviour can be observed in Fig. 25 for the SHS $50\times50\times3$-2 specimen loaded in the '1/3 span' configuration. In this case the moment ratio based on elastic analysis equals 1.875 and a higher degree of moment redistribution is necessary to form a plastic mechanism. The experimental results confirm the initially elastic distribution of bending moments and show significant redistribution towards equal moments at collapse. The evolution of the $M_{support}/M_{span}$ ratio (i.e. ratio of the moment at the support $M_{support}$ to the moment at span $M_{span}$) with increasing displacement can also be observed in Figs. 26 and 27 for the I-$200\times140\times10\times8$-1 and I-$200\times140\times10\times8$-2 specimens respectively, where the respective theoretical responses based on elastic-perfectly plastic analysis (with $M_{csm}$ in

**Table 11**
Assessment of the CSM for indeterminate structures.

| Specimen | Class | CSM for indeterminate structures | |
|---|---|---|---|
| | | $\varepsilon_{csm}/\varepsilon_y$ | $F_{pred}/F_u$ |
| SHS 50 × 50 × 3-1 | 1 | 10.5 | 0.91 |
| SHS 50 × 50 × 3-2 | 1 | 11.1 | 0.91 |
| SHS 60 × 60 × 3-1 | 1 | 8.9 | 0.93 |
| SHS 60 × 60 × 3-2 | 1 | 8.9 | 0.98 |
| SHS 100 × 100 × 3-1 | 4 | 1.1 | N/A |
| SHS 100 × 100 × 3-2 | 4 | 1.1 | N/A |
| RHS 60 × 40 × 3-MA-1 | 1 | 10.2 | 0.84 |
| RHS 60 × 40 × 3-MA-2 | 1 | 10.2 | 0.85 |
| RHS 60 × 40 × 3-MI-1 | 1 | 5.6 | 0.84 |
| RHS 60 × 40 × 3-MI-2 | 1 | 5.6 | 0.85 |
| I-200 × 140 × 6 × 6-1 | 4 | 1.2 | N/A |
| I-200 × 140 × 8 × 6-1 | 3 | 2.7 | N/A |
| I-200 × 140 × 10 × 8-1 | 1 | 8.5 | 0.91 |
| I-200 × 140 × 12 × 8-1 | 1 | 15.0 | 0.93 |
| I-200 × 140 × 6 × 6-2 | 4 | 1.2 | N/A |
| I-200 × 140 × 8 × 6-2 | 3 | 2.7 | N/A |
| I-200 × 140 × 10 × 8-2 | 1 | 8.9 | 0.95 |
| I-200 × 140 × 12 × 8-2 | 1 | 15.0 | 1.02 |
| Mean | | | 0.91 |
| COV | | | 0.06 |

**Table 12**
Comparison of test data reported by Mirambell and Real [4,5] with design predictions based on elastic analysis.

| Specimen | EN 1993-1-4 [2] | | Revised slenderness limits [15] | | CSM |
|---|---|---|---|---|---|
| | Class | $F_{pred}/F_u$ | Class | $F_{pred}/F_u$ | $F_{pred}/F_u$ |
| SHS 80 × 80 × 3 | 4 | 0.63 | 1 | 0.74 | 0.76 |
| SHS 80 × 80 × 3 | 4 | 0.68 | 1 | 0.80 | 0.82 |
| RHS 120 × 80 × 4 | 1 | 0.72 | 1 | 0.72 | 0.80 |
| RHS 120 × 80 × 4 | 1 | 0.72 | 1 | 0.72 | 0.80 |
| I 100 × 100 × 8 | 1 | 0.70 | 1 | 0.70 | 0.89 |
| I 100 × 100 × 8 | 1 | 0.70 | 1 | 0.70 | 0.89 |
| Mean | | 0.69 | | 0.73 | 0.83 |
| COV | | 0.05 | | 0.05 | 0.07 |

**Table 13**
Comparison of test data reported by Mirambell and Real [4,5] with design predictions based on plastic analysis.

| Specimen | Conventional plastic analysis based on EN 1993-1-4 (2006) | | Conventional plastic analysis based on revised slenderness limits | | CSM for indeterminate structures | |
|---|---|---|---|---|---|---|
| | Class | $F_{pred}/F_u$ | Class | $F_{pred}/F_u$ | $\varepsilon_{csm}/\varepsilon_y$ | $F_{pred}/F_u$ |
| SHS 80 × 80 × 3 | 4 | 0.63 | 1 | 0.83 | 2.0 | N/A |
| SHS 80 × 80 × 3 | 4 | 0.68 | 1 | 0.88 | 2.0 | N/A |
| RHS 120 × 80 × 4 | 1 | 0.81 | 1 | 0.81 | 4.6 | 0.89 |
| RHS 120 × 80 × 4 | 1 | 0.81 | 1 | 0.81 | 4.6 | 0.89 |
| I 100 × 100 × 8 | 1 | 0.79 | 1 | 0.79 | 14.2 | 1.00 |
| I 100 × 100 × 8 | 1 | 0.79 | 1 | 0.79 | 14.2 | 1.00 |
| Mean | | 0.75 | | 0.82 | | 0.95 |
| COV | | 0.10 | | 0.04 | | 0.07 |

place of $M_{pl}$) is also depicted. Initially the experimentally obtained moment–displacement curves follow an idealised elastic response, while under increasing loading, moment redistribution gradually occurs and the $M_{support}/M_{span}$ ratio decreases until collapse occurs. Overall, the theoretical model offers a good prediction of the observed response, particularly in relation to ultimate conditions.

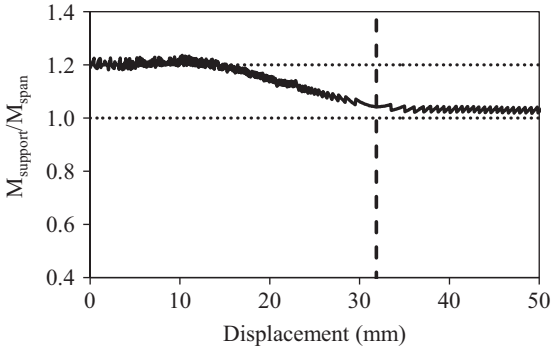


**Fig. 24.** Evolution of support to moment ratio with increasing displacement for SHS 50 × 50 × 3-1.

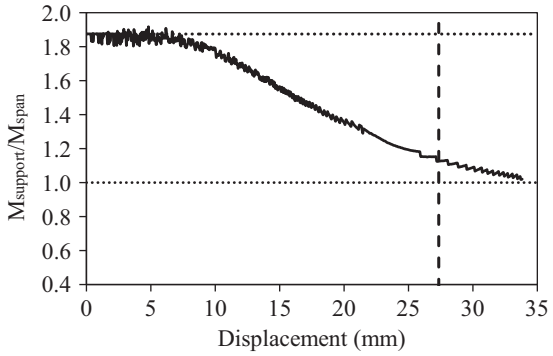


**Fig. 25.** Evolution of support to moment ratio with increasing displacement for SHS 50 × 50 × 3-2.

An additional assumption underpinning the CSM for indeterminate structures is that structural collapse occurs when the cross-sectional deformation capacity at the critical plastic hinge is reached. This implies a monotonic moment–rotation response for all plastic hinges and simplifies the design procedure. However, such an assumption may be overly conservative for some configurations and accounting for the softening branch of the moment–rotation response may be beneficial since the evolution of plasticity and strain-hardening at successive hinges and the corresponding increase in energy dissipation could increase the ultimate load. However, dealing with softening materials (or moment-rotation characteristics) can be complex, although some effective algorithms on the matter have been proposed [30] and applied successfully to continuous cold-formed steel purlins [31].

Based on the reported results and the accuracy of the predictions, the application of the CSM as modified for indeterminate structures is proposed herein for stainless steel indeterminate structures. Further research into the topic is underway, since improvements in design efficiency may be achieved if the proposed method is optimised on the basis of additional experimental and numerical results considering indeterminate structures with a higher degree of redundancy and more general loading conditions. Moreover, the adopted minimum deformation capacity values, beyond which CSM for indeterminate structures is applicable, should be reassessed on the basis of a larger data pool.

## 5. Conclusions

Following an experimental study comprising 13 three-point bending tests and 18 two-span continuous beam tests (five-point bending), the conservatism embedded in the provisions for stainless steel indeterminate structures codified in EN 1993-1-4 [1] has

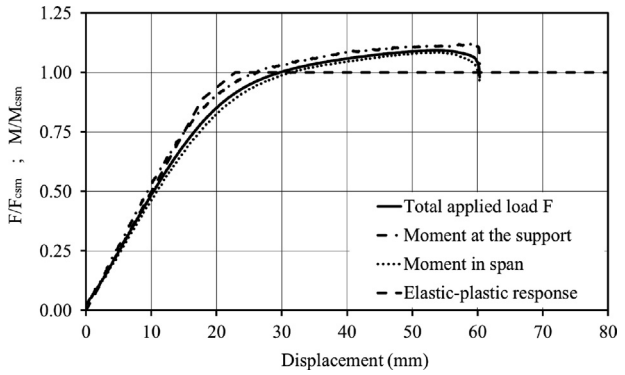


**Fig. 26.** Experimental and theoretical response of I-200 × 140 × 10 × 8-1 ('1/2 span configuration').

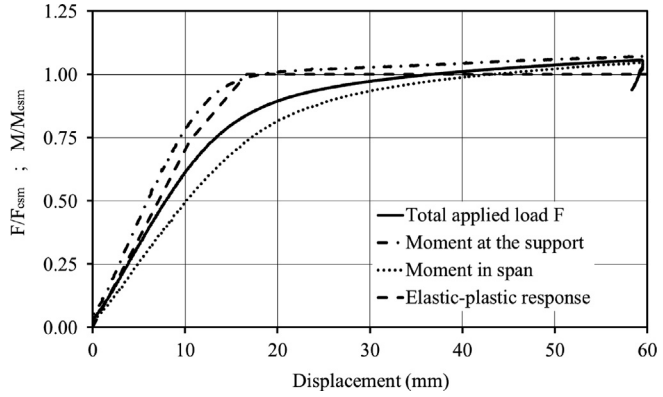


**Fig. 27.** Experimental and theoretical response of I-200 × 140 × 10 × 8-2 ('1/3 span configuration').

been highlighted. The application of conventional plastic analysis to stainless steel indeterminate structures and the accuracy of the CSM have been investigated and were found to only partially alleviate the conservatism embedded in [2]. It was concluded that both material strain-hardening at the cross-sectional level (at the location of the plastic hinges) and moment redistribution occurring in indeterminate structures, comprising sections with sufficient deformation capacity, are significant and should therefore be accounted for in design. A recently proposed adaptation of the CSM for carbon steel indeterminate structures has been further investigated and applied to stainless steel continuous beams, yielding excellent results for stocky cross-sections. However, additional research, both experimental and numerical, is still required in order to further optimise the method. In particular, the determination of suitable slenderness criteria and the possibility of incorporating the falling branch of the moment–rotation response into the method need to be further investigated. Moreover, the applicability of the proposed design method to more structural systems with a higher degree of redundancy and more general loading configurations should be assessed.

## References

[1] EN 1993-1-1. Eurocode 3: Design of steel structures – Part 1.1: General rules – General rules and rules for buildings. CEN; 2005.
[2] EN 1993-1-4. Eurocode 3: Design of steel structures – Part 1.4: General rules – Supplementary rules for stainless steel. CEN; 2006.
[3] Gardner L. The use of stainless steel in structures. Prog Struct Eng Mater 2005;7(2):45–55.
[4] Mirambell E, Real E. On the calculation of deflections in structural stainless steel beams: anexperimental and numerical investigation. J Construct Steel Res 2000;54(1):109–33.
[5] Real E, Mirambell E. Flexural behaviour of stainless steel beams. Eng Struct 2005;27(10):1465–75.
[6] Gardner L, Ashraf M. Structural design for non-linear metallic materials. Eng Struct 2006;28(6):926–34.
[7] Ashraf M, Gardner L, Nethercot DA. Structural stainless steel design: Resistance based on deformation capacity. J Struct Eng, ASCE 2008;134(3):402–11.
[8] Theofanous M, Gardner L. Effect of element interaction and material nonlinearity on the ultimate capacity of stainless steel cross-sections. Steel Compos Struct 2012;12(1):73–92.
[9] Theofanous M. Studies of the nonlinear response of stainless steel structures [PhD thesis]. Department of Civil and Environmental Engineering, Imperial College London; 2010.
[10] Saliba N. Structural behaviour of lean duplex stainless steel welded I-sections [PhD thesis]. Department of Civil and Environmental Engineering, Imperial College London; 2012.
[11] Saliba N, Gardner L. Cross-section stability of lean duplex stainless steel welded I-sections. J Construct Steel Res 2013;80(1):1–14.
[12] Nip KH, Gardner L, Elghazouli AY. Cyclic testing and numerical modelling of carbon steel and stainless steel tubular bracing members. Eng Struct 2010;32(2):424–41.
[13] EN 10002-1. Metallic materials – Tensile testing – Part 1: Method of test at ambient temperature, CEN; 2001.
[14] Rasmussen KJR. Full-range stress–strain curves for stainless steel alloys. J Construct Steel Res 2003;59(1):47–61.
[15] Gardner L, Theofanous M. Discrete and continuous treatment of local buckling in stainless steel elements. J Construct Steel Res 2008;64(11):1207–16.
[16] Lay MG, Galambos TV. Inelastic steel beams under uniform moment. J Struct Div, ASCE 1965;91(6):67–93.
[17] Lay MG, Galambos TV. Inelastic beams under moment gradient. J Struct Div, ASCE 1967;93(1):381–99.
[18] Ashraf M, Gardner L, Nethercot DA. Strength enhancement of the corner regions of stainless steel cross-sections. J Construct Steel Res 2005;61(1):37–52.
[19] Cruise RB, Gardner L. Strength enhancements induced during cold forming of stainless steel sections. J Construct Steel Res 2008;64(11):1310–6.
[20] Rossi B, Afshan S, Gardner L. Strength enhancements in cold-formed structural sections. Part II: Predictive models. J Construct Steel Res 2013;83:189–96.
[21] Schafer BW. Review: The Direct Strength Method of cold-formed steel member design. J Construct Steel Res 2008;64(7 and 8):766–78.
[22] Schafer, BW, Ádány S. Buckling analysis of cold-formed steel members using CUFSM: conventional and constrained finite strip methods. In: Eighteenth international specialty conference on cold-formed steel structures, Orlando, FL, October 2006.
[23] Li, Z & Schafer, BW. Buckling analysis of cold-formed steel members with general boundary conditions using CUFSM: conventional and constrained finite strip methods. In: Proceedings of the 20th International Specialty Conference on Cold-Formed Steel Structures, St. Louis, MO; November, 2010.
[24] EN 1993-1-5. Eurocode 3. Design of steel structures: part 1–5: plated structural elements. CEN; 2006.
[25] Gardner L, Wang FC, Liew A. Influence of strain hardening on the behaviour and design of steel structures. Int J Struct Stab Dyn 2011;11(5):855–75.
[26] Afshan S, Gardner L. The continuous strength method for structural stainless steel design. Thin-walled Struct 2013;68(1):42–9.
[27] Gardner L, Saari N, Wang F. Comparative experimental study of hot-rolled and cold-formed structural steel hollow sections. Thin-Walled Struct 2010;48(7):495–507.
[28] Bild S, Roik K, Sedlacek G, Stutzki C, Spangemacher R. The *b*/*t*-ratios controlling the applicability of analysis models in Eurocode 3, Part 1.1. Background Document 5.02 for chapter 5 of Eurocode 3, Part 1.1, Aachen; 1989.
[29] Sedlacek, G, Feldmann M. The *b*/*t*-ratios controlling the applicability of analysis models in Eurocode 3, Part 1.1. Background Document 5.09 for chapter 5 of Eurocode 3, Part 1.1, Aachen; 1995.
[30] Laine M, Tuomala M. Testing and design of gravity-loaded steel purlins restrained by sheeting. J Construct Steel Res 1999;49(2):129–38.
[31] Thomopoulos KT, Mistakidis ES, Koltsakis EK, Panagiotopoulos PD. Softening behaviour of continuous thin-walled steel beams. Two numerical methods. J Construct Steel Res 1996;36(1):1–13.